Chapter 4: Color Tunable Emission in a Hybrid of $CsPbBr_3$ with Europium Metal-Organic Framework for Anti-Counterfeiting Application

4.1 Introduction

The properties and challenges of the inorganic halide perovskite ($CsPbX_3$; X=Cl, Br, I) have been discussed in Chapter 1. To increase the stability of inorganic halide perovskite ($CsPbBr_3$), lanthanide ion (Eu^{2+}) has been doped into $CsPbBr_3$ and further their stability as well as different optical properties is discussed in Chapter 3. The Eu^{2+}-ion gives emission in the blue region along with characteristic green emission of $CsPbBr_3$. The stability of the Eu^{2+}-doped $CsPbBr_3$ get improved, uniform crystallinity is achieved and non-radiative emission also get reduced as compared to the pristine $CsPbBr_3$. The surface capping ligands such as oleic acid, oleylamine, metal-organic frameworks (MOFs), etc., encapsulate the $CsPbX_3$ and increase the stability of $CsPbX_3$.

Metal-organic frameworks (MOFs) are porous-crystalline materials formed by a metal cluster coordinated with organic linkers. The coordination between metal nodes and organic linkers delivers a high degree of chromophore because of different types of energy transfer mechanisms [165]. Further, the modeling of metal clusters, organic linkers, and external guest species can tailor the luminescent and photon-induced physical and chemical properties of MOFs [165][166][167]. Thus, the development of guest-modified luminescent MOFs have attracted lots of attention recently.

In modified MOFs, luminescence occurs through various processes e.g., organic linker-centered emission, metal-centered emission, induced charge transfer, and through guest-centered emission, etc., [165][166][167][168]. The organic-inorganic HPs $CH_3NH_3PbBr_3$ as a guest in lanthanide-based MOFs ($CH_3NH_3PbBr_3$@Eu-MOF) is reported with both metal-centered and guest-centered emission and used for thermal sensitivity and the anti-counterfeiting application [111]. However, the stability of $CH_3NH_3PbBr_3$ perovskite is less compared to the IHPs.

In this Chapter, we have synthesized an Eu-based MOF interfaced with $CsPbBr_3$ as a guest ($CsPbBr_3$@Eu-MOF) using the post treated hydrothermal method. The bi-flower like morphology of $CsPbBr_3$@MOF shows emission color variation in green – red region under different wavelength excitation. Hence, we have explored this material for the optical anti-counterfeiting application.

4.2 Materials Synthesis

4.2.1 Synthesis of Eu-MOF

The Eu-MOF is synthesized using the hydrothermal method. $Eu(NO_3)_3$ is obtained by the reaction of Eu_2O_3 (99.99 %, Alfa Aesar) and HNO_3 (Qualigens, 5 ppm). To obtain the 0.5 mmol of $Eu(NO_3)_3$, 0.25 mmol of Eu_2O_3 is taken in a beaker and the required amount of HNO_3 is added into it. The solution is stirred for 1 h at 200 rpm at a temperature of 40 ºC to obtain a clear transparent nitrate solution. Then, the temperature is increased to 120 ºC to remove the excess HNO_3. Further, 5 mL N, N-Dimethyle formamide (DMF, 99 %, EMPCURA) solution is added into it and stirred to obtain the clear transparent solution. In another beaker containing 15 mL of DMF, 0.5 mmol of 1,3,5 benzene-tricarboxylic acid (H_3BTC, 98%, Thermo Scientific) is added and stirred at 40 ºC for 1 h at 200 rpm to get a perfectly dissolved solution. Then, both the solutions (DMF solution of $Eu(NO_3)_3$ and H_3BTC) are mixed in a beaker and is ultra-sonicated for 10 mins to obtain a homogeneous mixture. This solution is then transferred into a Teflon-lined stainless steel autoclave and kept in a furnace at 120 ºC for 48 h [111]. Then, it is centrifuged at 7000 rpm and washed several times using ethanol (EOH, 99.9 %). Supernatant is discarded, and particles are dried in a vacuum oven maintained at 80 ºC for 12 h.

4.2.2 Synthesis of $PbBr_2$@Eu-MOF

For the synthesis of $PbBr_2$@Eu-MOF, the same synthesis steps and precursors are followed as for Eu-MOF discussed earlier, only an additional precursor lead bromide ($PbBr_2$, 99.998 %, Alfa Aesar) of 0.5 mmol is dissolved in 5 mL DMF solution.

4.2.3 Synthesis of $CsPbBr_3$@Eu-MOF

In $CsPbBr_3$@ Eu-MOF synthesis, 0.1 mmol of CsBr (99.999%, Alfa Aesar) is dissolved in 6 mL of methanol (MeOH, 99%, Qualigens) and 2 mL of deionized (DI) water kept at 40 ºC for 30 mins. Thus, obtained $PbBr_2$@Eu-MOF power is mixed in a beaker containing CsBr solution. The solution color changes from colorless to dark yellow color, which is an indication of the formation of $CsPbBr_3$. It is stirred for 10 mins at 40 ºC with 200 rpm for uniform mixing to get the $CsPbBr_3$@ Eu-MOF. Then, it is centrifuged at 7000 rpm and washed several times using EOH. Supernatant is discarded, and particles are dried in a vacuum oven maintained at 80 ºC for 12 h. Finally, the yellow color powder is obtained which is used for further characterization and analysis.

4.3 Results and Discussion

4.3.1 Structural and Morphology Analysis

The structure and phase of the synthesized Eu-MOF and $CsPbBr_3$ @ Eu-MOF have been analyzed by using XRD characterization. This is done with a step size of 0.02° and in the range of $10 \leq 2\theta \leq 90$, with the instrument Miniflex 600 diffractometer, Rigaku, Japan. The characteristic wavelength of the Cu Kα radiation source was utilized for the diffraction. The XRD patterns of the Eu-MOF, $PbBr_2$@Eu-MOF, and $CsPbBr_3$ @Eu-MOF are shown in Fig. 4.1(a-c), respectively. The diffraction peaks perfectly matched with the reported pattern, which is the validation of the formation of the Eu-MOF [169][170][171]. The Eu-MOF has a tetragonal structure with space group $P4_322$, as confirmed by the reported XRD pattern. Eu-atom is coordinated with the six oxygen atoms of the carboxylate group H_3BTC ligand in a tetragonal structure.

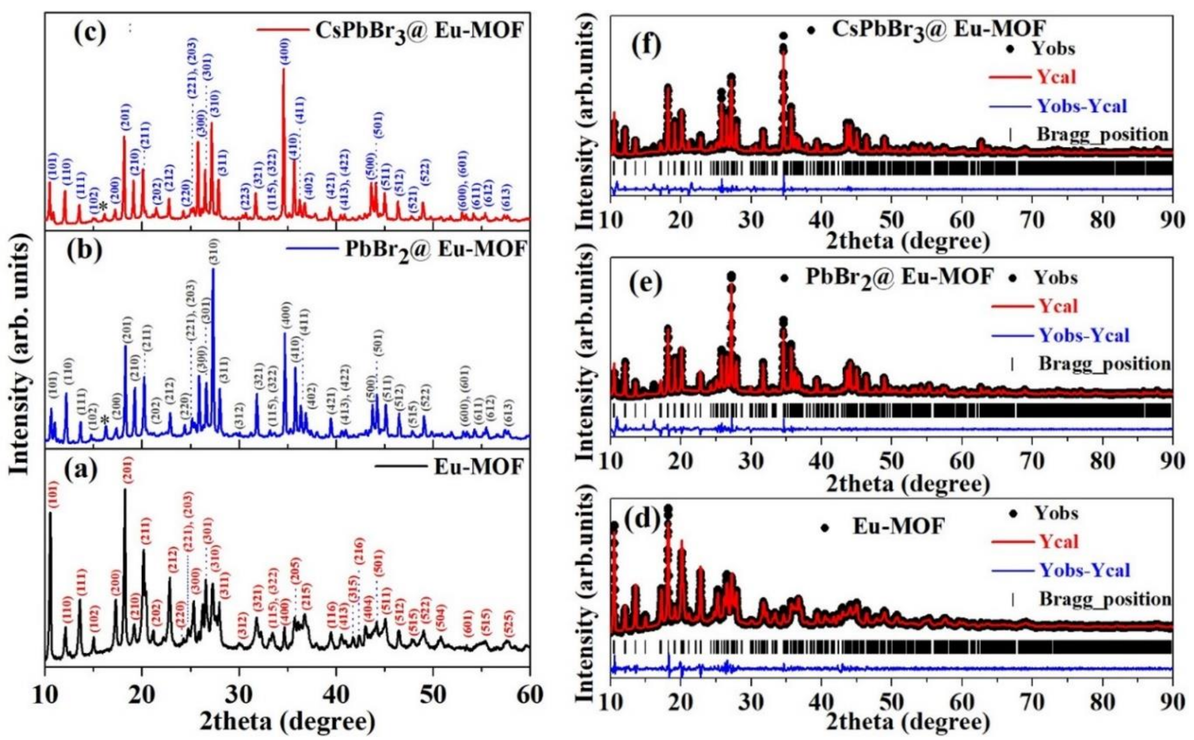

Figure 4.1: XRD patterns of (a) Eu-MOF, (b) $PbBr_2$@ Eu-MOF, and (c) $CsPbBr_3$@ Eu-MOF. LeBail fitted XRD patterns of (d) Eu-MOF, (e) $PbBr_2$@ Eu-MOF, and (f) $CsPbBr_3$@ Eu-MOF.

The XRD pattern of Eu-MOF shows the prominent peaks in the range 10° - 40° at 10.58°, 12.14°, 13.60°, 15.02°, 17.32°, 18.26°, 19.22°, 20.18°, 21.18°, 22.88°, 25.34°, 26.60°, 27.30°, 27.98°, 31.82°, 34.68°, 35.72°, 36.76°, and 39.48°. All these peaks are present in $PbBr_2$@Eu-MOF, and $CsPbBr_3$@Eu-MOF (see Fig. 4.1). The consistency in the XRD patterns of the $PbBr_2$@Eu-MOF and $CsPbBr_3$@Eu-MOF with the diffraction pattern of the Eu-MOF, indicate successful insertion of the $PbBr_2$ and hence $CsPbBr_3$ inside the Eu-MOF. The (hkl) indexing of the planes corresponding to the prominent diffraction peaks are shown for all the three samples. The intensity profile of the peaks slightly changes. Neither any extra diffraction peaks nor any shift in the peaks are observed in the XRD patterns of $PbBr_2$@ Eu-MOF and $CsPbBr_3$@ Eu-MOF in reference to the Eu-MOF. These reveal the structure and phase stability of the Eu-MOF after interfacing it with $CsPbBr_3$.

To obtain the unit cell parameters of the synthesized Eu-MOF, $PbBr_2$@ Eu-MOF, and $CsPbBr_3$@ Eu-MOF, “LeBail” fitting has been done using the “FullProf Suite” software. The peak shape function selected is “Pseudo-Voigt,” and the background type opted is “linear interpolation between a set of background points with refinable heights.” The selected refinement weighting model is “Least Squares”. The obtained unit cell and fitted parameters after the “LeBail” fitting is listed in Table 4.1.

Table 4.1 The lattice parameters of Eu-MOF, $PbBr_2$@ Eu-MOF, and $CsPbBr_3$@ Eu-MOF obtained by LeBail analysis.

Parameter	Eu-MOF	$PbBr_2$@ Eu-MOF	$CsPbBr_3$@ Eu-MOF
Phase	Tetragonal	Tetragonal	Tetragonal
Space group	$P4_322$	$P4_322$	$P4_322$
$\boldsymbol{a = b}$ **(Å)**	10.36182 ± 0.00047	10.36658 ± 0.00012	10.36199 ± 0.00009
$\boldsymbol{c}$ **(Å)**	14.40584 ± 0.00088	14.45335 ± 0.00080	14.40850 ± 0.00112
$\boldsymbol{\alpha = \beta = \gamma}$ **(°)**	90	90	90
Volume **(Å^3)**	1546.715 ± 0.138	1553.243 ± 0.090	1547.052 ± 0.122
Profile residual (*R*p)	2.48	3.07	3.16
Weighted profile residual (*R*wp)	3.49	5.75	5.60
Expected profile residual (*R*exp)	2.02	1.60	1.55

The tetragonal phase of the Eu-MOF is well retained after attaching $PbBr_2$ and $CsPbBr_3$ i.e. for $PbBr_2$@ Eu-MOF and $CsPbBr_3$@ Eu-MOF samples. Lattice parameters of the Eu-MOF are a = b = 10.36182 $\pm$ 0.00047 Å, c =14.40584 $\pm$ 0.00088 Å, and $\alpha = \beta = \gamma = 90°$. These parameters slightly increased in $PbBr_2$@ Eu-MOF, and it is a = b = 10.36658 $\pm$ 0.00012 Å, and c =14.45335 $\pm$ 0.00080 Å. This is due to the microstructure parameters such as change in crystallite size and random lattice strain induced in the Eu-MOF hydrocarbon chain molecule resulting due to percolation of foreign molecule $PbBr_2$, etc. For the $CsPbBr_3$@Eu-MOF, the parameters are a = b = 10.36199 $\pm$ 0.00009 Å, and c =14.40850 $\pm$ 0.00112 Å. The lattice parameters slightly get reduced in comparison to the $PbBr_2$@ Eu-MOF. It is expected due to mitigated stress caused due to the formation of stable structured $CsPbBr_3$ inside the Eu-MOF.

The morphology study of the as-synthesized Eu-MOF and $CsPbBr_3$@ Eu-MOF was carried out by the field emission scanning electron microscopy (FE-SEM) (model Nova Nano SEM 450, USA). The Eu-MOF has a beautiful bi-flower morphology shown in Fig. 4.2(a) and 4.2(b). In bi-flower morphology, the middle portion length is 5-7 μm, whereas the conical part of the bi-flowers lies between 47 μm. Bi-flower is formed by the uniform, well-defined square rods of square edge~length 200 nm, shown in Fig. 4.2(c). Morphology of the $CsPbBr_3$@ Eu-MOF is like a square-rod. The length of the well-defined rod morphology lies in the range of 30–100 μm with thickness variation 5–10 μm, as shown in Fig. 4.2(d).

However, this requires MOF growth-kinetics study and interaction among the metal-ions, guest-center and organic linker to correlate the morphology transformation. Elemental mapping of $CsPbBr_3$@Eu-MOF has been done by energy-dispersive X-ray analysis. The mapping of the Eu, Cs, Pb, and Br is depicted, respectively in Fig. 4.2(e), 4.2(f), 4.2(g), and

4.2(h) and is the validation of the presence of all constituent elements in the synthesized samples.

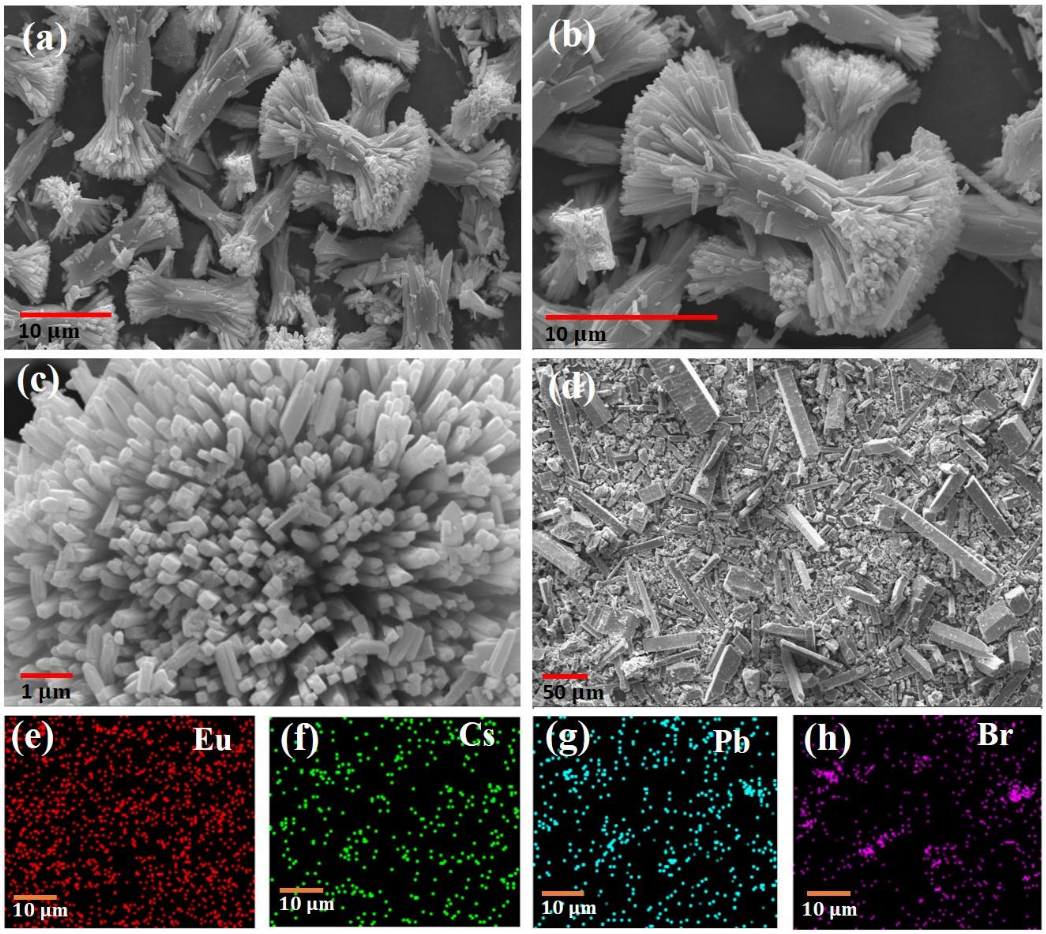

Figure 4.2: FE-SEM images of (a, b) Eu-MOF, (c) top view of the Eu-MOF flower like morphology, (d) $CsPbBr_3$@Eu-MOF. Elemental mapping of the elements (e) Eu, (f) Cs, (g) Pb, and (h) Br in $CsPbBr_3$@Eu-MOF.

4.3.2 UV-visible NIR Absorption Analysis

UV-visible NIR absorption spectra of crystalline Eu-MOF, $PbBr_2$@Eu-MOF, and $CsPbBr_3$@ Eu-MOF are recorded by JASCOV770 spectrophotometer, spectra are shown in Fig. 4.3. The spectra of all these samples show a broad peak between 295–314 nm (having maxima at 295 nm in Eu-MOF, 300 in $CsPbBr_3$@Eu-MOF, 314 nm in $PbBr_2$@Eu-MOF), which is the prominent absorption peak of organic linker H_3BTC used in Eu-MOF synthesis.

Further, Eu-MOF, and $PbBr_2$@Eu-MOF show sharp and well-defined absorption peaks at 360, 395, 415, 465, and 535 nm. The broad and shoulder peak at about 360 nm comprises two absorption transition $^7F_{0,1} \rightarrow {}^5D_4$ due to Eu^{3+} ion. Other sharp peaks are assigned as: the peak at 395 nm corresponds to $^7F_0 \rightarrow {}^5L_6$ transition, 415 nm to the $^7F_0 \rightarrow {}^5D_3$, 465 nm to the $^7F_0 \rightarrow {}^5D_2$, 535 nm to the $^7F_1 \rightarrow {}^5D_1$ and 591 nm to the $^7F_1 \rightarrow {}^5D_0$ transition of Eu^{3+} ion.

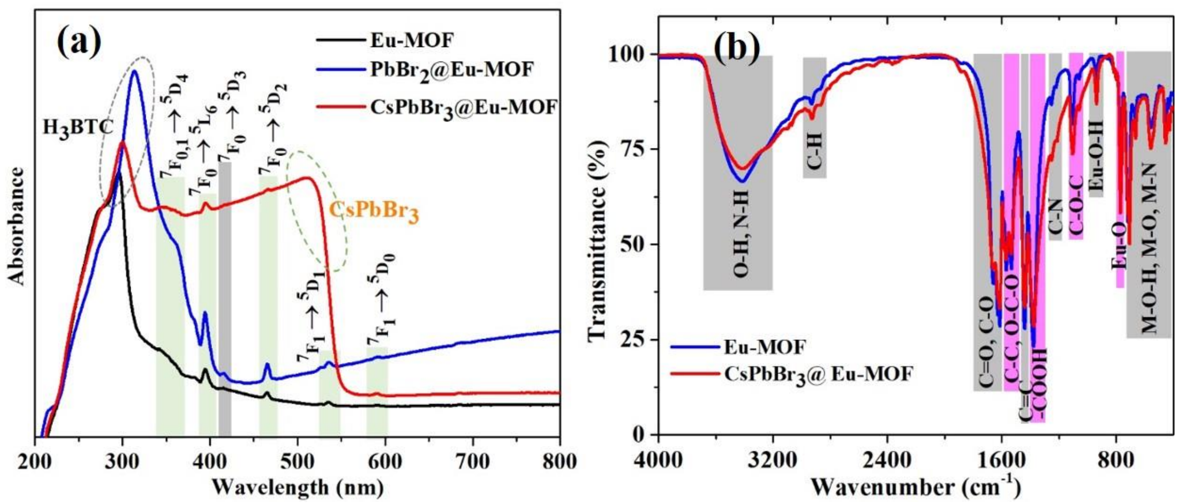

Figure 4.3: UV-visible absorption spectra of Eu-MOF, $PbBr_2$@Eu-MOF and $CsPbBr_3$@Eu-MOF. (b) FT-IR spectra of Eu-MOF and $CsPbBr_3$@Eu-MOF.

$CsPbBr_3$@Eu-MOF also shows characteristic absorption peaks at 360, 395, 415, and 465 nm. However, in addition to these peaks, the $CsPbBr_3$@Eu-MOF absorption spectrum has a very sharp absorption edge (indicated in a dotted closed curve) at about 508 nm. This is the characteristic absorption of the $CsPbBr_3$. Due to the sharp absorption edge of the $CsPbBr_3$, the 535 nm absorption peak of Eu-atom gets suppressed (see Fig. 4.3: #$CsPbBr_3$@Eu-MOF). The significant change in the absorption spectrum of $CsPbBr_3$@Eu-MOF compared to the Eu-MOF and $PbBr_2$@Eu-MOF indicates a successful formation of $CsPbBr_3$ inside the Eu-MOF [172].

4.3.3 Fourier Transform Infrared (FT-IR) Study

Fourier transform infrared (FT-IR) spectroscopy was performed in the range 400 – 4000 cm^{-1} by the Nicoleti S5 Thermofisher setup to determine the functional groups present in the sample. FT-IR spectra of the Eu-MOF and $CsPbBr_3$@Eu-MOF are shown in Fig. 4.3(b). The peaks and pattern of both the samples are same with only a small variation in the intensity of the bands. A broad peak at 3415 cm^{-1} is contributed by the water (H-O-H) adsorbed on the surface [173]. In between 3100 – 2800 cm^{-1}, peaks are symmetric and asymmetric stretching vibration peaks of the C-H [174]. The peak at 2928 cm^{-1} is due to the stretching vibration of CH_2 and the peak at 2865 cm^{-1} is due to the bending vibration of CH_2 [175]. Many well-defined peaks appear in the range 1850 – 400 cm^{-1}. The peak at 1650 cm^{-1} is due to the C-O stretching vibration present in the DMF molecule and also due to the hydroxyl group (O-H) [173][79]. The C = O vibration is responsible for the peak at 1614 cm^{-1} [176]. H_3BTC contains a benzene ring, which defines C-C skeleton vibration at 1570 cm^{-1} [177]. This peak also corresponds to the carboxylic group C-O-C asymmetric stretching. The peak at 1440 cm^{-1} is due to the C=C vibration in the aromatic ring. The symmetric and asymmetric vibration of the carbonyl group (-COOH) present in the MOF is ascribed by the peak appearing at 1377 cm^{-1} [178]. The peak at 1213 cm^{-1} is the C-N stretching vibration [174]. These two peaks are also due to the CH_3 skeletal vibration and out-of-plane bending vibration of C=C–H. The peak due to C-O-C stretching vibration appears at 1059 cm^{-1} [79]. It is reported that the peaks between 830-725 cm^{-1} are also due to the C-H vibrations present in different functional groups and inorganic compounds [176]. It also reflects the characteristic bond vibration peak in the fingerprint region (below 1000 cm^{-1}) in the FTIR spectrum. The Eu-O characteristics stretching vibration is assigned by the peak at 770 cm^{-1} [179]. The possible vibration corresponding the prominent peaks observed in the FTIR spectra of Eu-MOF and $CsPbBr_3$@Eu-MOF are listed in Table 4.2. Many significant peaks in the fingerprint region, such as 707, 664, 558, 454, and 426 cm^{-1}, are expected due to the metal-oxygen-hydrogen (M -O-H), metal-oxygen (M - O), metal-nitrogen (M - N), etc., bond vibrations [111][180]. However, this assignment requires further confirmatory study.

Table 4.2 Vibrational peaks observed in the FTIR spectrum of Eu-MOF and $CsPbBr_3$@Eu-MOF and their assignments.

Vibrational Energy (cm^{-1})	**Vibrational modes**
3415	N–H, O–H stretching vibration, H-O-H surface adsorbed
2928	CH_2 stretching vibration
2865	CH_2 bending vibration
1658	C-O stretching vibration, O-H hydroxyl group
1614	C = O vibration
1570	C-C stretching vibration, C-O symmetric and asymmetric stretching, O-C-O asymmetric stretching
1440	C=C aromatic ring
1377	-COOH symmetric and asymmetric vibrations
1213	C-N stretching, C=C–H out-of-plane bending,
1059	C-O-C stretching vibration
937	Eu-O-H vibration
770	Eu-O stretching vibration, C-H vibration

4.3.4 Photoluminescence (PL) Study

Photoluminescence (PL) study was performed by Horiba Fluorolog-3 spectrophotometer. A 450W xenon lamp is used as the excitation source, and a photomultiplier tube (PMT) is the detector. The photoluminescence excitation spectrum of $CsPbBr_3$@Eu-MOF, recorded for the emission peak at 615 nm (Eu^{3+}), is shown in Fig. 4.4(a). In the excitation spectrum, prominent peaks appear at 326, 361, 366, 374, 380, 386, 395, 415, 464, 525, 536, 555, 589, and 591 nm. All the peaks are well-matched with the reported spectrum of Eu^{3+} [181]. The peak at 326 nm arises due to the transition from $^7F_0 \rightarrow {}^5H_3$, peak at 361 nm for the transition $^7F_0 \rightarrow {}^5D_4$, peak at 366 nm due to $^7F_1 \rightarrow {}^5D_4$, peaks at 374 nm and 380 nm for the transition $^7F_0 \rightarrow {}^5G_3$ and $^7F_0 \rightarrow {}^5G_2$, respectively. Similarly, the peak at 386 nm for $^7F_0 \rightarrow {}^5L_7$, 395 nm for the $^7F_0 \rightarrow {}^5L_6$, 415 nm for the $^7F_0 \rightarrow {}^5D_3$, 464 nm for the $^7F_0 \rightarrow {}^5D_2$, 525 nm for the $^7F_0 \rightarrow {}^5D_1$, 536 nm for the $^7F_1 \rightarrow {}^5D_1$, 555 nm for the $^7F_2 \rightarrow {}^5D_1$, 589 nm for the $^7F_0 \rightarrow {}^5D_0$, and 591 nm for the transition $^7F_1 \rightarrow {}^5D_0$ transitions of Eu^{3+}-ion [182][183]. Various transitions in Eu^{3+}-ion that contribute to the excitation peaks discussed above are depicted in the energy level diagram shown in Fig. 4.5(b). Among all these transition peaks, the 395 nm peak is the most intense and excites the sample very efficiently relative to other excitation peaks. The excitation spectrum of the $CsPbBr_3$@Eu-MOF is also recorded for the 508 nm characteristic emission of $CsPbBr_3$. It shows broad excitation in the range of 300 – 430 nm, as shown in inset of Fig. 4.4(a). This clearly suggests the incorporation of $CsPbBr_3$ crystal inside the Eu-MOF, i.e., the formation of the $CsPbBr_3$@Eu-MOF.

There are various mechanisms to show luminesce phenomena in the MOF. The organic linker may give intra-ligand emission, ligand-to-metal charge transfer (LMCT) emission, and metal-to-ligand charge transfer (MLCT) emission [169]. The lanthanide ions in the organic framework give sharp emission and are an indication of the formation of MOF. The emission intensity of the lanthanide ion may increase through the antenna effect played by the organic linker used to form MOF [184]. In addition, if the entrapped guest is a luminescence molecule in the MOF, it also gives its characteristic emission.

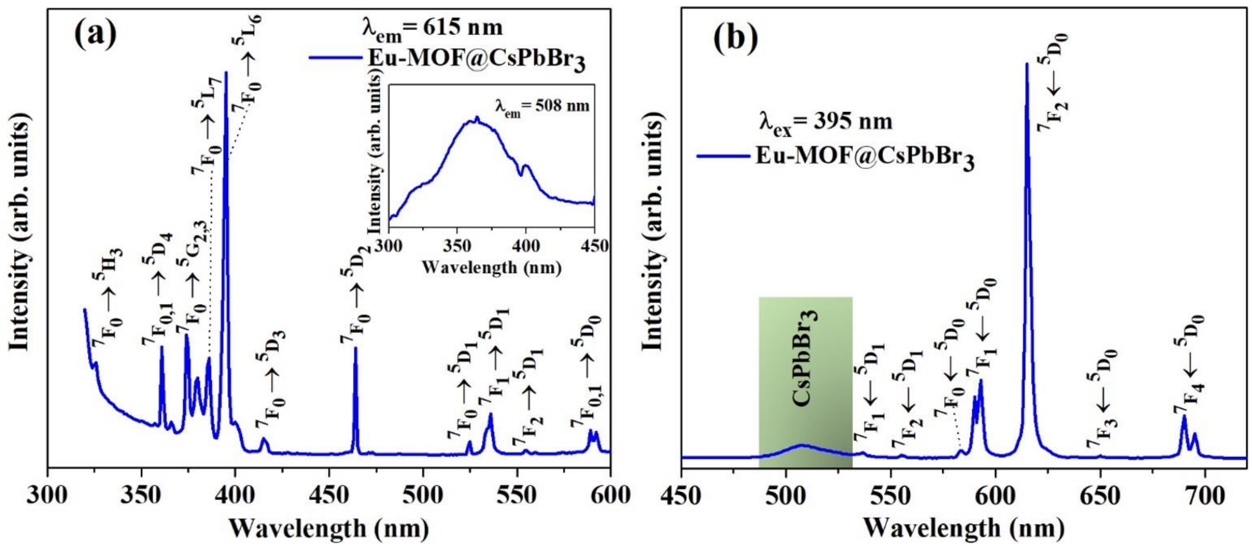

Figure 4.4: (a) Excitation spectrum of $CsPbBr_3$@Eu-MOF monitored for the emission wavelength 615 nm. The inset shows the excitation spectrum of $CsPbBr_3$@Eu-MOF monitored for the emission wavelength at 508 nm. (b) Emission spectrum of $CsPbBr_3$@Eu-MOF for λ_{exc}= 395 nm.

The emission spectrum of $CsPbBr_3$@ Eu-MOF is recorded by illuminating the sample with the most intense excitation peak at the wavelength of 395 nm. The emission spectrum of $CsPbBr_3$@ Eu-MOF is shown in Fig. 4.4(b). Eu^{3+} containing MOF structure gives emission pattern mainly due to the transitions from the $^5\mathrm{D}_0 \rightarrow {}^7\mathrm{F}_J$, i.e. from the excited level $^5\mathrm{D}_0$ to the different J (J = 0, 1, 2, 3, 4, 5 and 6) values of the ground level $^7\mathrm{F}_J$ [77]. The emission spectrum of $CsPbBr_3$@Eu-MOF consists of the peaks at 537, 555, 583, 593, 615, 650, and 690 nm. Transition from $^5\mathrm{D}_1 \rightarrow {}^7\mathrm{F}_1$ in Eu^{3+} appears at 537 nm while the peak at 555 nm corresponds to the transition $^5\mathrm{D}_1 \rightarrow {}^7\mathrm{F}_2$. The peak at 593 nm corresponds to the magnetic dipole transition $^5\mathrm{D}_0 \rightarrow {}^7\mathrm{F}_1$ of the Eu^{3+} ion, while the peak at 615 nm is due to the induced electric dipole (ED) transition $^5\mathrm{D}_0 \rightarrow {}^7\mathrm{F}_2$, 650 nm peak due to the $^5\mathrm{D}_0 \rightarrow {}^7\mathrm{F}_3$ ED transition, 690 nm peak due to the $^5\mathrm{D}_0 \rightarrow {}^7\mathrm{F}_4$ ED transition. All these transitions are indicated in the energy level diagram shown in Fig. 4.5(b). Among these emission peaks of the Eu^{3+}-ion, 615 nm emission is the most intense peak (see Fig. 4.4(b). In addition to the above-discussed peaks, one broad emission peak centered at 508 nm also appears in $CsPbBr_3$@Eu-MOF. This is the characteristic emission band of the CsPbBr$_3$ and is an indication of the successful interfacing of CsPbBr$_3$ crystal with the Eu-MOF structure.

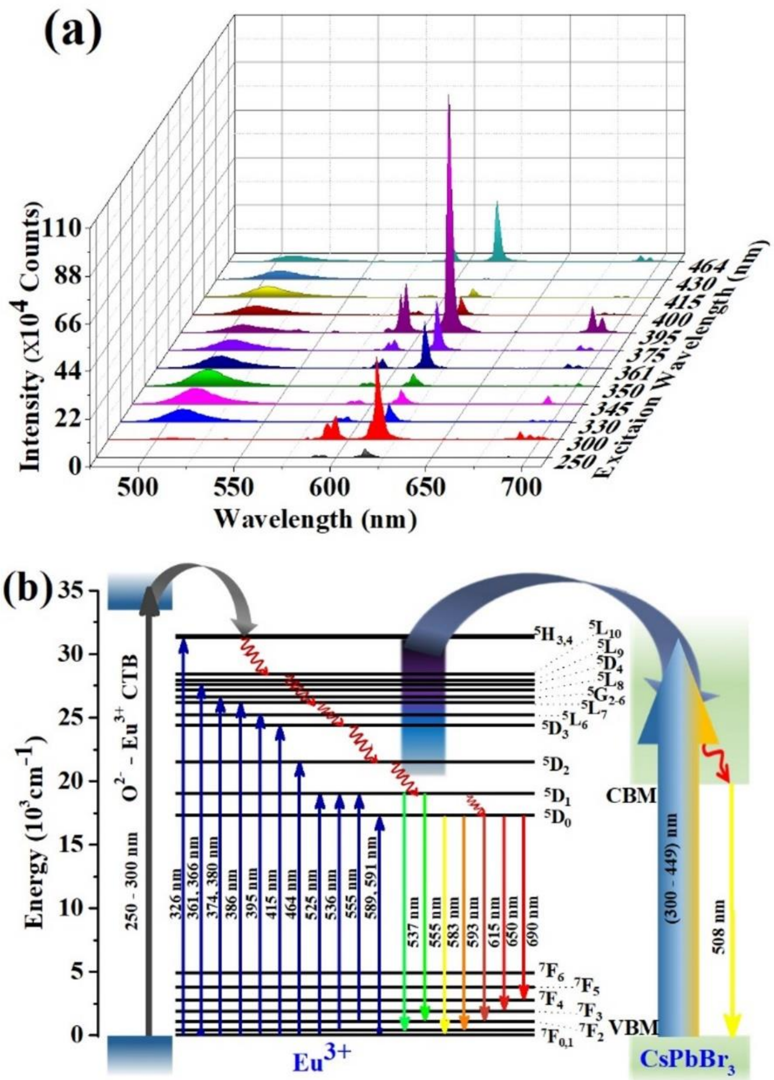

Figure 4.5: (a) PL spectra of CsPbBr$_3$@Eu-MOF for various excitation wavelengths. (b) Partial energy level diagram of Eu^{3+} indicating excitation/emission transitions and possible sensitization schemes in CsPbBr$_3$@Eu-MOF**.**

Further, we have also recorded the emission spectra of the CsPbBr$_3$@Eu-MOF by various other excitation wavelengths such as 250, 300, 330, 345, 350, 361, 375, 395, 400, 415, 430, and 464 nm. Three categories of excitation wavelength were selected to see the energy-transfer scheme between CsPbBr$_3$ and Eu-MOF in the CsPbBr$_3$@ Eu-MOF structure.

These are: (i) full centered excitation wavelengths that include 361, 395, 415, and 464 nm; (ii) slightly off-centered excitation wavelengths that are 330 and 400 nm; and (iii) highly off-centered wavelengths 250, 300, 345, 350, and 430 nm. The emission pattern for the centered and off-centered excitation wavelengths remains the same for all the excitations, with intensity variation as shown in Fig. 4.5(a). Among highly off-centered wavelengths: the excitation of $CsPbBr_3$@ Eu-MOF with 250, 300, and 430 nm gives very selective emission. Excitation in the range 250-300 nm is supported by a charge transfer band (CTB) formed by the O^{2-} (2*p* orbital) and Eu^{3+} (4*f* orbital) [185][186]. It is observed that characteristic emission of $CsPbBr_3$ is absent for the excitation at 250 nm and significantly weak emission for the 300 nm excitation (see Fig. 4.7(a) and 4.7(b)). However, the characteristic emission of Eu^{3+} at 615 nm is highly intense. On the contrary, 430 nm excitation only gives characteristic intense emission of $CsPbBr_3$. From these observations, we can predict that the self-sensitization of Eu^{3+} ion in the organic framework also activates the $CsPbBr_3$ (see Fig. 4.5(b)) [168].

4.3.5 Commission International de I′ Eclairage (CIE) Chromaticity study

As reported earlier by many research groups, the CIE 1931 coordinates depend on the host, type of doping ion, concentration of doping ion, etc. [79][109][187]. The PL spectra of the $CsPbBr_3$@Eu-MOF show significant variation in emission peaks under different excitation wavelengths. These comprise perception of different colors by the eyes under excitation with different wavelengths. Therefore, we calculated the color coordinates (x, y) of emission spectra of the $CsPbBr_3$@Eu-MOF using Commission International de I′ Eclairage (CIE)-1931 to support the color variation by the excitation wavelength. The CIE chromaticity diagram of $CsPbBr_3$@ Eu-MOF is shown in Fig. 4.6. The obtained CIE 1931 color coordinates (x, y) and luminous efficacy of the optical radiation (LER) are listed in Table 4.3. The emission's color purity (CP), an important concern for the color LEDs and display application, is also calculated [79]. The obtained *CP* values are listed in Table 4.3.

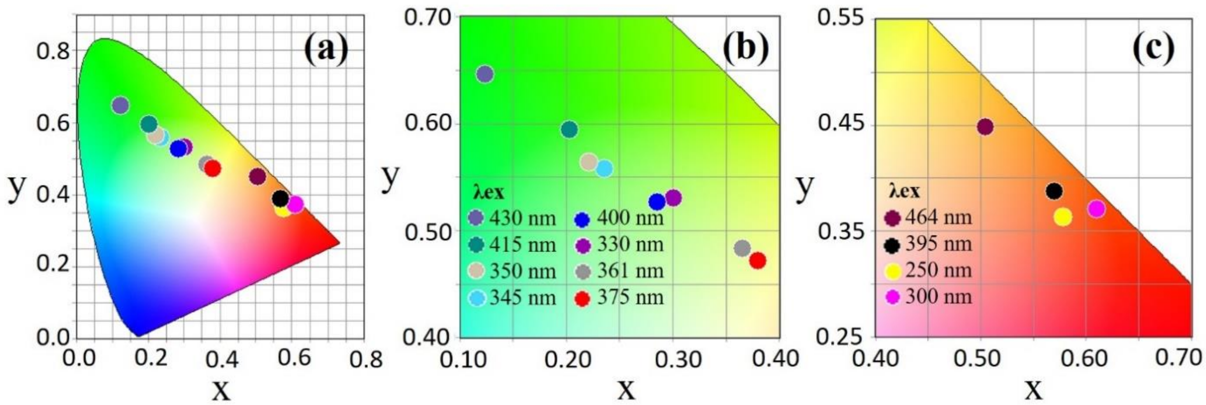

Figure 4.6: (a) CIE chromaticity diagrams of $CsPbBr_3$@Eu-MOF for different excitation wavelengths. Integrated CIE chromaticity diagram of $CsPbBr_3$@Eu-MOF for the excitation wavelengths (b) 330, 345, 350, 361, 375, 400, 415, and 430 nm; (c) 250, 300, 395, and 464 nm.

Table 4.3 CIE coordinates, LER, and color purity of the emission of $CsPbBr_3$@Eu-MOF for different excitation wavelengths.

Excitation Wavelength (nm)	CIE (x, y) coordinates	LER (lm/W)	Color Purity (%)
250	(0.5782, 0.3634)	301	82.6
300	(0.6104, 0.3705)	320	94.4
330	(0.3008, 0.5305)	338	50.8
345	(0.2362, 0.5580)	334	45.9
350	(0.2217, 0.5637)	340	46.1
361	(0.3655, 0.4830)	334	54.9
375	(0.3802, 0.4716)	334	55.8
395	(0.5702, 0.3877)	319	87.5
400	(0.2855, 0.5270)	346	46.0
415	(0.2030, 0.5940)	352	52.1
430	(0.1240, 0.6465)	359	68.4
464	(0.5049, 0.4486)	339	86.3

The CIE 1931 color coordinates for the emission from $CsPbBr_3$@Eu-MOF varies from green to red region. The excitation with 330, 345, 350, 361, 375, 400, 415, and 430 nm wavelengths gives the CIE color coordinate in the green region, as shown in Fig. 4.6(b). It covers the whole green region starting from the CIE 1931 (x, y) value (0.3008, 0.5305) for 430 nm excitation wavelength and extends up to (0.3802, 0.4716) for the 375 nm which is close to the red region. Whereas the excitation with the wavelengths 250, 300, 395, and 464 nm gives CIE 1931 color coordinates (x, y) in the red region (see Fig. 4.6(c)) in between (0.5049, 0.4486) for the 464 nm and (0.6104, 0.3705) for the 300 nm excitation. The LER values lie between 301 to 359 lm/W, minimum for 250 nm excitation wavelength and maximum for 430 nm. The CP is very important for color LEDs and display applications [79]. The maximum CP obtained is 94.4% for 300 nm excitation wavelength, and the minimum is 45.9 %. Thus, the CIE study reveals that this material can be used for the color LEDs and display applications in the green-red regions with considerably good CP by the selective excitation wavelength.

4.3.6 Optical Anti-Counterfeiting Application

In this era of rapidly increasing industries and manufacturing bodies, fraudulent and replicating any product is a significant concern. Original products, documents, logos/identification marks, and currency notes are replicated frequently, leading to human health issues and risks for the company or brand's reputation, economy, and society. Optical features like holograms, micro-printing, and diffraction patterns are widely used to mitigate fraud risk. However, these techniques are costly and require sophisticated instrumentation for generating patterns. Optical anti-counterfeiting is one of the simplest and cheapest techniques. Many researchers and scientific groups developed various kinds of phosphor materials, such as single structure, core@ shell, composite, MOF, etc., for anti-counterfeiting applications [179][188][189][190][191]. These include multi-wavelength stimuli, multi-color emission, dynamic responsiveness, and multi-stage anti-counterfeiting. Multi-wavelength, dynamic responsive, and multi-stage anti-counterfeiting are reported in a multi-structure frame. However, multi-color emission through selective excitation in a single matrix has not been reported so far to the best of our knowledge.

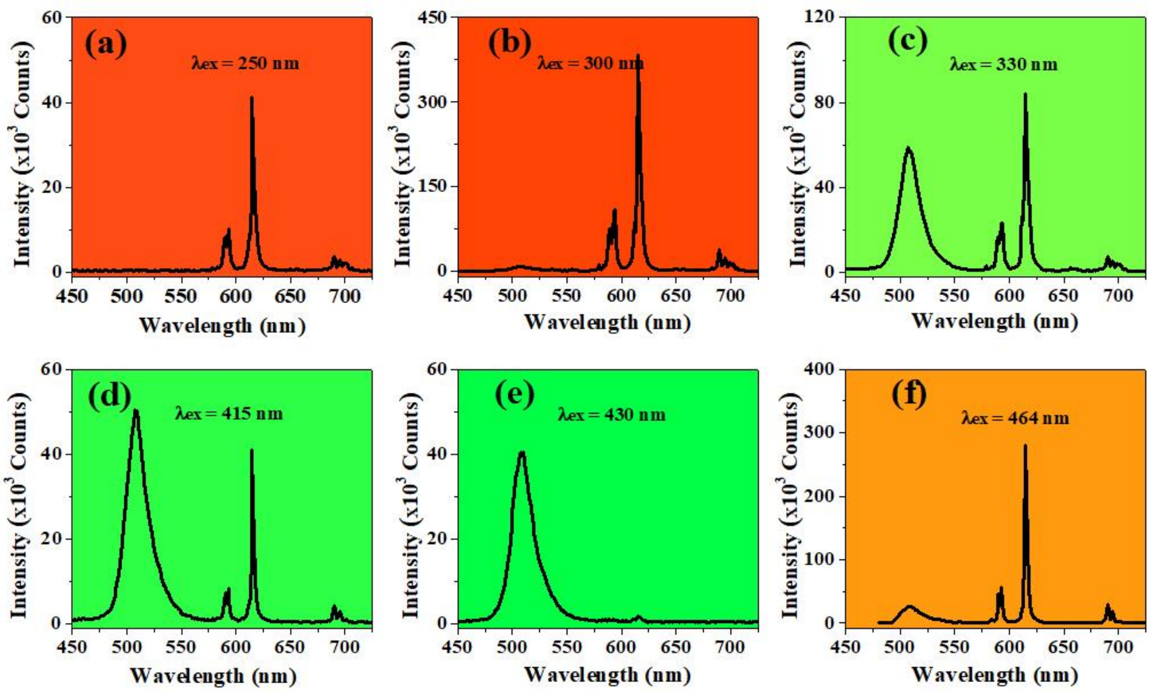

Figure 4.7: PL emission spectra of $CsPbBr_3$@Eu-MOF under various excitation wavelengths selected for anti-counterfeiting study.

Herein, we have demonstrated multi-color emission in a single $CsPbBr_3$@Eu-MOF matrix. The $CsPbBr_3$@Eu-MOF is mixed with a PMMA matrix using acetone as a solvent. Using this mixed matrix, we have encrypted the pattern "LMDD" on white paper ("LMDD" – W), on butter paper ("LMDD" – B), on green plastic ("LMDD" – G), and on aluminum foil ("LMDD" – A) substrate. The patterns are illuminated in the light ranging from UV to visible. These include daylight, in UV-regions under 250, 300, and 330 nm, and in the visible region illuminated wavelengths are 415, 430, and 464 nm. The PL spectra of $CsPbBr_3$@ Eu-MOF corresponding to these excitation wavelengths are shown in Fig. 4.7. The PL spectra peaks intensity variation by the excitation wavelength gives a cumulative effect of color change to the eye.

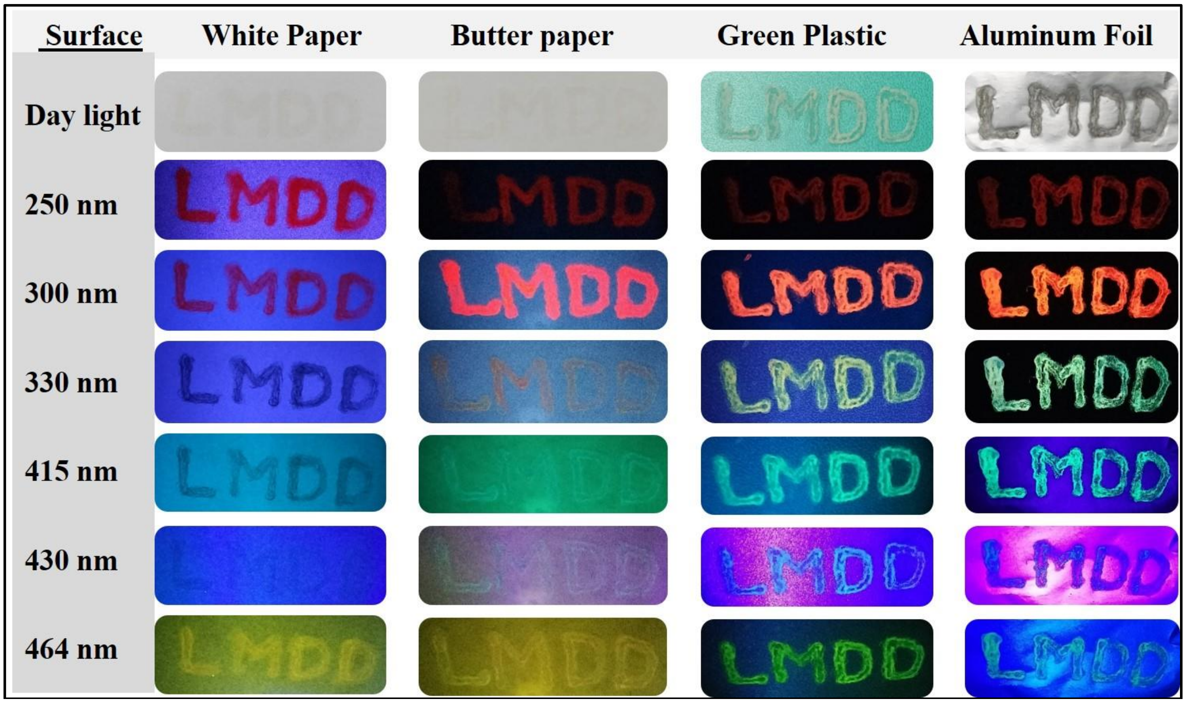

Figure 4.8: Encrypted "LMDD" patterns on different surfaces and the appearance of the patterns under different wavelength light illumination.

Digital photographs of the encrypted patterns exposed under the daylight, 250, 300, 330, 415, 430, and 464 nm are shown in Fig. 4.8. The encrypted pattern "LMDD" – W does not show much intense color variation when changing the illumination wavelength. In this case, the substrate surface on which patterns are encrypted also shows weak emission of similar color when light is illuminated. The substrate emission mixed with the encrypted pattern emission creates a problem of distinct color appearance from the pattern "LMDD" - W. Thus, the substrate selection on that pattern or code to be encrypted is vital for encryption-decryption applications. When the encrypted pattern is seen in the daylight, it is much less visible for the “LMDD” – B. Although the encrypted patterns on the “LMDD” – G and “LMDD” – A are seen through the naked eye, the patterns are colorless. Under 250 nm irradiation, the color of all the encrypted patterns, “LMDD,” appears intense red, while by 300 nm light, the patterns are orange-red. The color intensity is maximum for the “LMDD” – A. For 300 nm wavelength, the color intensity of the “LMDD” – G is slightly less than the “LMDD” – A, and the intensity of the “LMDD” – B is slightly less than the “LMDD” – G. On 330 nm wavelength illumination, the pattern “LMDD” – W reflects greyish-blue, while “LMDD”- B light-orange-red. On the other hand, the color appearance of the “LMDD”- G and “LMDD”- A on 330 nm wavelength light is cyan. The patterns “LMDD”- W and “LMDD”- B show faint bluish-gray color on 415 nm wavelength irradiation, while “LMDD”- G and “LMDD”- A show blue color. The color appearance of the encrypted pattern “LMDD”- W on 464 nm wavelength is mustard-yellow, “LMDD”- B appears lime-green, “LMDD”- G is green, and “LMDD”- A is whitish. Pattern encrypted on green plastic shows a more intense green color than the patterns encrypted on other substrate surfaces. Among all the encrypted patterns, “LMDD”- G and “LMDD”- A show good color appearance upon the incident wavelengths selected for the illumination. Hence, this material is very suitable for optical encryption and decryption when the pattern or code is encrypted on plastic-like and metal surfaces. The digital photographs of the patterns “LMDD”- G and “LMDD”- A are recorded after 300 nm light illumination 60 days later from the day of encryption of the pattern “LMDD” to see the environmental stability of the pattern. The captured digital photographs of “LMDD”- G and “LMDD”- A are shown in Fig. 4.9(a) and (b), respectively. The physical appearance, intensity, and color of both the patterns remain almost the same as the infant one. This reflects the good environment stability of the encrypted patterns "LMDD"- G and "LMDD"- A.

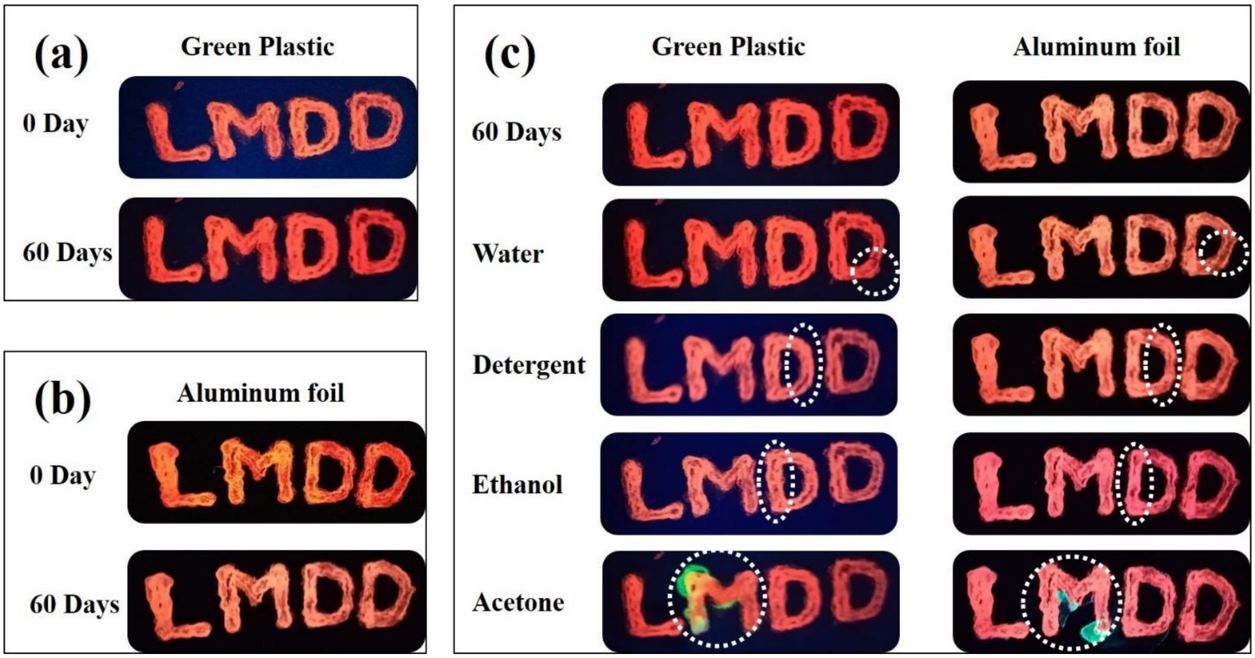

Figure 4.9: Digital photographs of the pattern "LMDD" encrypted on (a) green plastic and (b) aluminum foil on 0^{th} and 60^{th} days from the time of encryption, after exposure by 300 nm wavelength, (c) Digital photographs of the pattern "LMDD" after dropping different solutions (water, detergent, ethanol, and acetone) on the indicated portion of the pattern (irradiation wavelength is 300 nm).

For the chemical stability test of the encrypted patterns ("LMDD"- G and "LMDD"- A), we encountered it with solutions such as, water, detergent, ethanol, and acetone. The portion of the "LMDD" pattern that encounters the solution is marked in the digital photograph captured after 300 nm wavelength irradiation, as shown in Fig. 4.9(c). The encrypted patterns "LMDD"- G and "LMDD"- A show no physical color and intensity change for the water, detergent, and ethanol. By acetone, the physical state of the encrypted pattern "LMDD" started to destroy, as indicated in the marked circle in Fig. 4.9(c). This is due to the dissolution of poly(methyle methacrylate) (PMMA) in ethanol. However, the intensity and color of the patterns remain almost the same. Thus, the proposed material shows multi-color emission from a single structure by changing the excitation wavelength.

Different stability tests show that encrypted patterns “LMDD”- G and “LMDD”- A are quite stable in an open environment and chemically stable for water, detergent, and ethanol. These studies reveal that this material can be a good anti-counterfeiting material, especially for plastic currency notes and metal-surface substrates.

4.4 Conclusions

We have successfully interfaced an IHPs ($CsPbBr_3$) with a lanthanide metal organic frame work (Eu-MOF) and developed a hybrid material $CsPbBr_3$@ Eu-MOF. It has a tetragonal structure with space group $P4_322$, confirmed by the XRD “LeBail” analysis. Synthesized Eu-MOF has bi-flower morphology whose mid portion and conical part length both are below 10 μm. The conical part of the bi-flower consists of many squared rods of square size 200 nm. Presence of the characteristic absorption edge, PL emission of $CsPbBr_3$, as well as elemental analysis using SEM-EDX, confirm successful formation of the $CsPbBr_3$@Eu-MOF. Excitation wavelength-dependent PL emission of $CsPbBr_3$@Eu-MOF shows variation in the emission peak intensity, that results in a change in cumulative color, which makes it a promising candidate for different applications. The (x, y) coordinate covers the whole green to red region in the CIE 1931 diagram. The maximum LER value achieved is 359 lm/W, and the maximum color purity is 94.4% which is significant for optical applications. Further, a pattern “LMDD” is encrypted on four different substrates (white paper, butter paper, green plastic, and aluminum foil) and the color change of the “LMDD” patterns under different excitation wavelengths has been thoroughly studied. The overall visualization and the chemical stability of the encrypted patterns on green plastic [“LMDD”-G] is the best among all the four substrates studied.